Available online at www.sciencedirect.com
SCIENCE DIRECT
Journal of Chromatography A, 1092 (2005) 114–124
JOURNAL OF CHROMATOGRAPHY A
www.elsevier.com/locate/chroma

Binding *Aedes aegypti* densonucleosis virus to ion exchange membranes

Binbing Han [a], Rachel Specht [a], S. Ranil Wickramasinghe [a,*], Jonathan O. Carlson [b]

[a] *Department of Chemical Engineering, Colorado State University, Fort Collins, CO 80523-1370, USA*
[b] *Department of Microbiology, Immunology & Pathology, Colorado State University, Fort Collins, CO 80523-1682, USA*

Available online 18 July 2005

Abstract

Experimental and numerical results for binding *Aedes aegypti* densonucleosis virus (AeDNV) using anion and cation exchange membranes are presented. AeDNV particles are adsorbed by anion and cation exchange membranes providing the virus particles and membranes are oppositely charged. Q membranes which are strongly basic anion exchangers were the most effective. Dynamic and static capacities for Q membranes were found to be similar. A numerical model is proposed which assumes a log normal pore size distribution. By estimating the required parameters from static binding experiments, the model may be used to calculate the breakthrough curve for virus adsorption.

Keywords: Adsorptive membranes; *Aedes aegypti* densonucleosis virus; Ion exchange membrane; Membrane chromatography

1. Introduction

Virus capture is critical in a number of applications. In gene therapy and vaccine production, large-scale purification of virus vectors is often essential. In the manufacture of biopharmaceuticals, validation of virus clearance is critical. Viruses are generally 5–300 nm in size. Many virus particles are larger than DNA and other biomolecules.

Packed-bed chromatography has been used for virus clearance [1–4] as well as virus purification [5–8]. In packed-bed chromatography, the solute in a feed solution is transported between the resin particles (usually spherical) by convective flow. Since chromatographic particles are usually porous, the majority of the binding sites are located on the surface of the internal pores. To reach these pores, the solute must diffuse from the bulk feed solution across a liquid film layer at the particle surface and into the pores. Next, the solute diffuses by "pore diffusion" through the pores and attaches to binding sites on the pore surface [9].

Berthold et al. [1] investigated ion exchange and affinity chromatography for clearance of model viruses. Valdés et al. [2] investigated the removal of sendaivirus, HIV-IIIb, Human herpesvirus I, Human poliovirus type II and canine parvovirus using protein A affinity chromatography. Roberts et al. [3] obtained 10^4 clearance of enveloped Sindbis virus and non-enveloped hepatitis A virus by metal chelate affinity chromatography. Kim et al. [4] studied various model viruses and a number of different removal methods. For Q-Sepharose resin based chromatography, 1.5–2.5 log removal of bovine herpes virus, bovine viral diarrhoea virus, murine encephalomyocarditis virus and porcine parvovirus were obtained.

Although these studies indicate the feasibility of virus removal by packed-bed chromatography, packed bed chromatography suffers from a number of limitations. The pressure drop across the bed is generally high and tends to increase during operation due to media deformation. Pore diffusion is often slow leading to increased processing time and possible degradation of fragile biological product molecules [10–14]. Scale up of packed beds is often difficult. Further, packed beds have been shown to display very low dynamic capacities for virus particles [15–17], leading to underutilized beds as most of the binding sites in the resin pores are not used.

Stacks of adsorptive membranes, as novel chromatographic supports, may overcome these limitations. Adsorptive microporous membranes have surface functional groups attached to the internal pores. The feed is pumped through the

* Corresponding author. Tel.: +1 970 491 5276; fax: +1 970 491 7369.
E-mail address: wickram@engr.colostate.edu (S.R. Wickramasinghe).

0021-9673/$ – see front matter © 2005 Elsevier B.V. All rights reserved.
doi:10.1016/j.chroma.2005.06.089

membrane pores; thus, transport of the solute to the binding sites occurs predominantly by convection, rather than pore diffusion. Thus the processing time can be greatly reduced. The pressure drop for flow through adsorptive membranes is significantly lower than for packed beds, as the flow path is much shorter, even for a stack of multiple membranes. Importantly, handling and scale-up of ready-to-use membrane devices is much easier than packing and scale-up of packed beds [9,10,18,19]. Thus adsorptive membranes may be ideally suited for virus capture and purification. Though previous researchers have considered capture of large biomolecules such as plasmid DNA and proteins, relatively few systematic studies report results for virus capture using ion exchange membranes.

Yang et al. [20] recently showed that for Q Sepharose beads, the dynamic capacity of a large protein molecule (thyroglobulin, 20 nm diameter) decreased rapidly with flow rate while that of a small protein molecule (α-lactalbumin, 3.5 nm diameter) was less sensitive to flow rate. By contrast, for Q membranes, the dynamic capacity for large proteins was the same as the static capacity. Knudsen et al. [21] also showed that for packed beds, due to hindered pore diffusion, the dynamic capacity is a strong function of flow rate for resin particles. However, anion exchange membranes exhibited a flow rate independent dynamic capacity over a large range of flow rates for binding of DNA and host cell proteins (Chinese hamster ovary cell protein, or CHOP). Further, the breakthrough capacities of ion-exchange membranes are often comparable in magnitude to ion exchange resins.

In a recent study, Teeters et al. [22] determined the capacity of commercially available anion-exchange membranes (Mustang-Q membranes, Pall BioPharmaceuticals, Pensacola, FL) for purification of plasmid DNA. Unlike anion-exchange resins, the dynamic capacity of the membranes was found to be independent of flow rate over a large range of flow rates. Further, the membrane capacity was found to be 10 mg mL^{-1}, twice the capacity reported by Levy et al. [23] for highly porous resins and five times greater than the capacity for 15 μm particles [22,23].

Heber et al. [24] studied binding of ∼7 kb long supercoiled DNA using Mustang Q ion exchange membranes. They also compared results for membranes and resins. They found that the dynamic capacity depended on flow rate for membranes and resins as the DNA elongated at higher flow rates. Nevertheless, the membranes exhibited a higher dynamic capacity than resin particles.

These studies demonstrate that adsorptive membranes may be ideally suited for virus capture. Here we have investigated the feasibility of adsorption of *Aedes aegypti* densonucleosis virus (AeDNV) particles using Sartobind (Sartorius AG, Göttingen, Germany) anion and cation exchange membranes. AeDNV is a mosquito specific parvovirus (non-enveloped, single-stranded DNA virus). The virus particles are about 20 nm in size, icosahedral in shape with an isoelectric point (p*I*) of 5.6. The virus is stable over the pH range 1–12.

We have chosen to investigate the binding of AeDNV since this virus is of practical significance and is a good model virus for studying binding to anion and cation exchange membranes. AeDNV is a parvovirus that infects the *Aedes aegypti* mosquito. The *Aedes aegypti* mosquito is a carrier of viruses that are human pathogens which cause dengue and yellow fever. Consequently development of an AeDNV vector may find important applications in integrated vector-borne disease control programs against human pathogens such as dengue and yellow fever [25].

AeDNV is a parvovirus very similar in size to minute virus of mice (MVM). MVM is a FDA recommended model parvovirus frequently used for validation of virus clearance. Validation of parvovirus clearance is particularly problematic. Further since AeDNV is stable above and below its isoelectric point, by adjusting the pH of the feed stream above and below the isoelectric point of the virus, binding of negatively and positively charged virus particles using anion and cation exchange membranes may be investigated. Many enveloped viruses such as human influenza virus and murine leukemia virus (also a FDA model virus for validation of virus clearance) are not stable at their isoelectric point. Thus binding of these viruses by cation and anion exchange membranes can not be investigated.

2. Materials and methods

2.1. Production of AeDNV particles

AeDNV particles were produced using a cell culture technique and mosquito larvae. In the cell culture method, AeDNV particles were produced by transfecting the *A. albopictus* cell line C6/36 with pUCA, an infectious clone containing the AeDNV genome [26]. The C6/36 cell line was grown at 28 °C in Leibovitz's L-15 medium supplemented with 10% fetal bovine serum and 1% penicillin-streptomycin (Invitrogen Co., Carlsbad, CA). The pH was 7.4. Transfection was performed in T-75 flasks with cells 80% confluent. The media was changed 8 to 18 h post transfection to remove the pUCA plasmid. Four days post transfection the T-75 flasks were frozen and thawed three times then centrifuged at 3750 rpm for 15 min at 4 °C to remove cellular debris. AeDNV particles produced by the cell culture technique are referred to as virus in growth medium.

AeDNV particles were also produced by exposing newly hatched *A. aegypti* larvae to transducing particles by introducing them into previously infected water containing AeDNV [27]. The larvae were grown in 28 °C water that contained a 50/50% mixture of tetra fin goldfish flakes and mouse and rat food at a concentration of 0.5 mg/mL water. Pupae and mosquitoes were removed by centrifugation at 3750 rpm for 15 min at 4 °C. The virus water solution was then filtered through a 0.22 μm filter (Millipore, Bedford, MA). AeDNV particles produced using mosquito larvae are referred to as AeDNV in water.

2.2. RT-PCR assay

A real time-PCR (RT-PCR) based assay was used to determine the virus titre in the infective solutions as AeDNV does not show cytopathic effects. The primers and probe were designed within a conserved region of the viral NS1 gene. Primer Express® oligo design software (Applied Biosystems, Foster City, CA) was used to design forward primer: CAT ACT ACA CAT TCG TCC TCC ACA A, reverse primer: CTT GCT GAT TCT GGT TCT GAC TCT T, and TaqMan Probe: FAMCCA GGG CCA AGC AAG CGC CTAMRA. The reaction was performed in 96-well format skirted v-bottomed polypropylene microplates (MJ Research, Inc., Waltham, MA) with optical caps (Applied Biosystems, Foster City, CA).

The Brilliant® multiplex QPCR master mix (Stratagene, La Jolla, CA) was used as the RT-PCR master mix. Each well consisted of 4 μL of unknown sample or standard control DNA pUCA plasmid, 0.3 μL of 0.002 mmol/L dye, 9.7 μL master mix, 2 μL of 0.05 mmol/L forward primer, 2 μL of 0.05 mmol/L reverse primer, and 2 μL of 5×10^{-3} mmol/L probe. The thermal cycling conditions were: stage 1, 50 °C for 2 min, stage 2, 95 °C for 10 min, stage 3, 95 °C for 15 s, stage 4, 60 °C for 1 min and then stages 3 and 4 repeated 39 times. All reactions were performed in the Opticon 2 DNA Engine (MJ Research, Inc., Waltham, MA). All samples were analyzed three times and average results are reported. The accuracy of the PCR assay was determined by analyzing 12 samples of the same infective solution and found to be within ± 0.5 log units.

A RT-PCR based method was used for the quantification of AeDNV virus since more conventional biological assays are not straightforward [28]. The quantitative RT-PCR assay is a rapid, sensitive and efficient way to compare samples. Though similar results could be obtained with naked viral genomic DNA, when batches of AeDNV prepared from cell culture or mosquito larvae as described in the manuscript are exposed to pancreatic DNase prior to RT-PCR, there is little or no reduction in signal. Also RT-PCR on pellet fractions after ultracentrifugation under conditions that should pellet virus particles indicates that most of the DNA is pelleted. These results give us confidence that we are measuring DNA from virus particles in these preparations rather than DNA from plasmid transfections or replicative forms.

2.3. Ion exchange experiments

All ion exchange experiments were conducted in triplicate at 20 °C. All results represent the average of the three runs. Ion exchange membranes consisting of strong and weak anion and cation exchange groups were obtained from Sartorius AG. Table 1 gives details of these regenerated cellulose membranes. The membrane modules consisted of 15 flat sheet membranes, 25 mm diameter, 275 μm thick and nominal pore size larger than 3 μm. The total membrane surface area was 75 cm^2. All membranes were tested using two feed streams: virus particles suspended in growth medium obtained by cell culture and virus particles suspended in water obtained using mosquito larvae. Experiments were conducted at different feed pH values by adding HCl or NaOH.

Membranes were initially rinsed with TE buffer (10 mmol/L Tris, 1 mmol/L EDTA, pH 7.0) at a flow rate of 1 mL/min. Next 10–50 mL of feed suspension was introduced at a flow rate of 1 mL/min. The membranes were then washed using 5–25 mL of TE buffer at a flow rate of 1 mL/min. Next the bound virus particles were eluted using 5–25 mL 0.5 mol/L NaCl solution at a flow rate of 1 mL/min. The virus titre in the permeate was determined by collecting 100 μL samples for RT-PCR analysis at regular intervals. Finally the membranes were regenerated using 25–50 mL 1 mol/L NaCl solution. The membranes were stored wet in a 1 mol/L KCl solution containing 20% ethanol.

Static binding capacity and association rate experiments were conducted by cutting Q membranes into small pieces of surface area 25 cm^2. These membranes were incubated in 20 mL of water containing AeDNV (produced using mosquito larvae) at pH 7.0. The suspension was gently stirred at 290 rpm at 28 °C. The change in virus titre in the suspension was determined by removing 100 μL samples at regular intervals for RT-PCR analysis.

3. Model description

Several models have been proposed to predict breakthrough curves for membrane chromatography. Suen and Etzel [29] developed a model to predict the breakthrough curves for affinity membranes. This model is modified here in order to describe the observed breakthrough of AeDNV using ion exchange membranes.

3.1. General model

The membranes used contain a pore size distribution. Further the pores are not straight but follow a tortuous path through the membrane. In addition the pores are interconnected. It is assumed that the pore size distribution can be

Table 1
Details of ion exchange membranes

Membrane	pK_a	Functional groups	Membrane charge	Comments
Q	11	R–CH_2–N^+–$(CH_3)_3$	pH < 11, positive	Strongly basic anion exchanger
D	9.5	R–CH_2–N–$(C_2H_5)_2$	pH < 9.5, positive	Weakly basic anion exchanger
S	1	R–CH_2–SO_3^-	pH > 1, negative	Strongly acidic cation exchanger
C	4.5	R–COO^-	pH > 4.5, negative	Weakly acidic cation exchanger

described by the log normal distribution. The effects of pore tortuosity and connectivity are combined into a tortuosity parameter, τ. For straight non connected pores, $\tau = 1$. In general $\tau > 1$. It is also assumed that a pore may be described by a single diameter, d.

Fig. 1 shows a schematic of a typical membrane pore. The axial direction, z, is from the top to the bottom surface of the membrane, i.e., feed solution with velocity V_0 and virus concentration x_F, flows in at the axial position $z = 0$. A differential volume of height dz at position z is taken as a control volume. The velocity of the liquid phase at position z is V_z. The pore diameter is d (radius r) and the membrane thickness is H. Since the pores are not straight, the real length of the liquid flow path is τH.

The rate of virus accumulation in the liquid within the control volume for a differential time dt is $dx\,\pi r^2\,dz$. The rate of accumulation depends on: (1) convection into the control volume from position z, $(Vx)_z\,\pi r^2\,dt$ where x is the concentration of the virus at position z, mol/m^3; (2) convection out of the control volume from position $z + dz$, $(Vx)_{z+dx}\,\pi r^2\,dt$; (3) axial diffusion into the control volume from position z, $-(E\partial x/\partial z)_z\,\pi r^2\,dt$, where E is the diffusion coefficient of the virus; (4) diffusion out of the control volume at position $z + dz$, $-(E\partial x/\partial z)_{z+dz}\,\pi r^2\,dt$; (5) the change of virus concentration in the liquid within the control volume due to adsorption onto ion exchange sites on the pore surface, $R_z\,\pi r^2\,dz dt$, where R_z is the rate of virus adsorption. In the 3rd and 4th terms the negative sign indicates that diffusion is from high concentration to low concentration.

It is assumed that adsorption of the virus V onto the ligand S on the membrane pore surface is given by the equation,

$$V + S \leftrightarrow VS \tag{1}$$

Eq. (1), which represents a second order reversible rate expression with a Langmuir isotherm, is clearly a major simplification as it is likely virus adsorption involves interactions with more than one ligand. Further the ligands are unlikely to act totally independently. Given the large size of virus particles, steric hindrance effects are likely to lead to many unavailable binding sites. In assuming Eq. (1) we are implying that a second order reversible rate expression will give an empirical description of the rate of adsorption and desorption of virus particles. Eq. (1) provides no information on the mechanism of adsorption. The rate constants for adsorption and desorption are k_a and k_d. Consequently,

$$R = \frac{\partial c_{VS}}{\partial t} = k_a x c_S - k_d c_{VS} \tag{2}$$

where c_s and c_{vs} represent the concentration of free ion exchange groups and the concentration of the virus–ion exchange group complex. The total number of ion exchange sites or maximum capacity of the membrane is given by c_l where,

$$c_l = c_S + c_{VS} \tag{3}$$

Note c_s, c_l and c_{vs} are all based on the pore surface area and have units of mol/m^2.

According to the mass conservation law,

$$\begin{aligned} dx\,\pi r^2 dz = {} & (Vx)_z\,\pi r^2\,dt - (Vx)_{z+dz}\,\pi r^2\,dt \\ & - \left(E\frac{\partial x}{\partial z}\right)_z \pi r^2\,dt + \left(E\frac{\partial x}{\partial z}\right)_{z+dz} \pi r^2\,dt \\ & - (k_a x c_S - k_d c_{VS})\,\pi r^2\,dz dt \end{aligned} \tag{4}$$

Dividing both sides of Eq. (4) by $dt dz$ and taking the limit as dt and dz go to zero,

$$\frac{\partial x}{\partial t} = -\frac{\partial (Vx)}{\partial z} + \frac{\partial (E(\partial x/\partial z)_z)}{\partial z} - (k_a x c_S - k_d c_{VS}) \tag{5}$$

Assuming the velocity V and virus diffusion coefficient E are independent of position z, Eq. (5) simplifies to,

$$\frac{\partial x}{\partial t} = -V\frac{\partial x}{\partial z} + E\frac{\partial^2 x}{\partial z^2} - (k_a x c_S - k_d c_{VS}) \tag{6}$$

3.2. Boundary conditions

Fig. 2 is a schematic representation of the top surface of the membrane. At this surface, the virus concentration changes

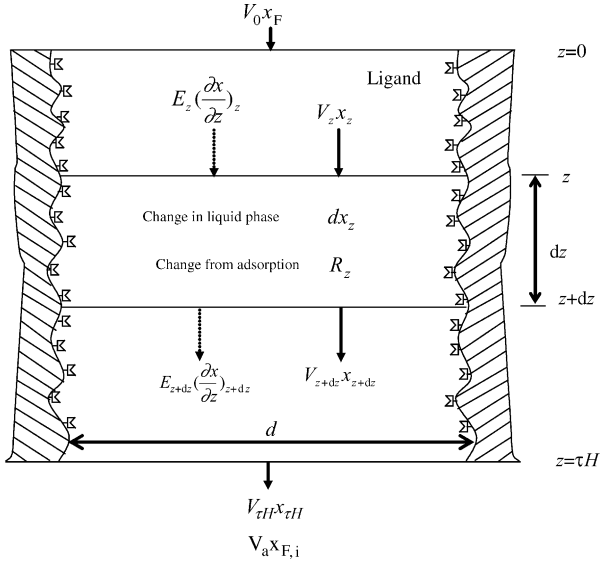

Fig. 1. Schematic diagram of a membrane pore.

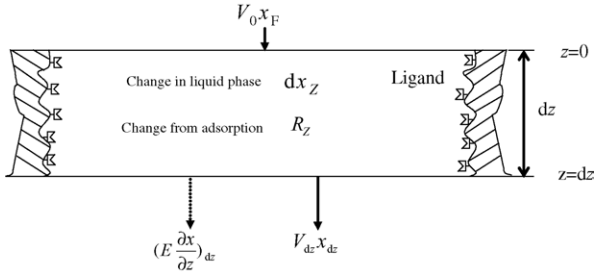

Fig. 2. Schematic representation of the top boundary of the membrane.

sharply due to axial mixing, i.e., virus concentration in the aqueous phase change from x_F to x_0. At the top surface of the membrane,

$$0 = Vx_F - Vx_0 + E\left(\frac{\partial x}{\partial z}\right)_0 \quad \text{at } z = 0, \quad t > 0 \tag{7}$$

Fig. 3 shows the bottom boundary of the membrane. The bottom boundary condition is,

$$0 = \left(\frac{dx}{dz}\right)_{\tau H} \quad \text{at } z = \tau H, \quad t > 0 \tag{8}$$

3.3. Initial conditions

At $t = 0$, the virus concentration in all the membrane pores is zero; the concentration of virus–ion exchange group complex on all the pore surfaces is also zero; and the free ion exchange group concentration is equal to the maximum concentration of ion exchange groups. Thus,

$$x = 0 \quad \text{at } t = 0 \tag{9}$$

$$c_{VS} = 0 \quad \text{at } t = 0 \tag{10}$$

$$c_S = c_l \quad \text{at } t = 0 \tag{11}$$

By solving Eqs. (2), (3) and (6)–(11) using the fourth order Runge-Kutta method, the concentration of virus in the liquid and adsorbed on to the membrane can be calculated. The virus associated parameters needed for the numerical simulation were obtained from the static binding capacity results. The membrane associated parameters needed for the numerical simulation were obtained from SEM images. The concentration of virus in the exit stream from the membrane module as a function of time, i.e., the breakthrough curve, can be obtained by averaging the concentration at $z = \tau H$ for all the pores at the bottom surface of the membrane. Using these parameters the model may be used to determine the breakthrough curve for virus particles.

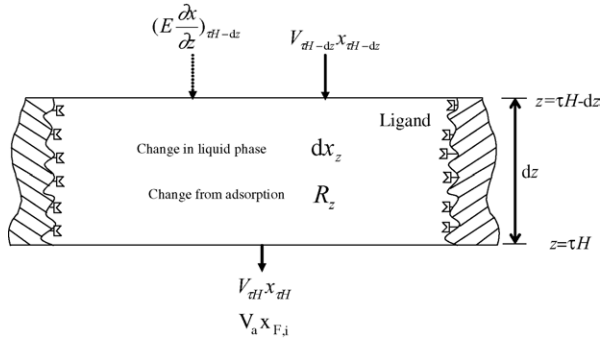

Fig. 3. Schematic representation of the bottom boundary of the membrane.

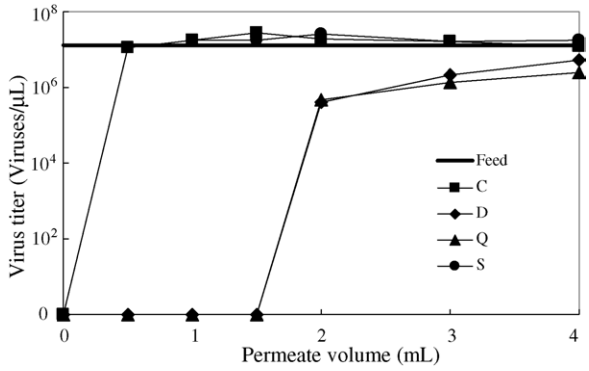

Fig. 4. Variation of the virus titre in the permeate with permeate volume. The feed consisted of virus particles suspended in growth medium at pH 7.0. The feed flow rate was 1.0 mL/min. Results are shown for C, D, Q and S membranes.

4. Results

Experimental breakthrough curves at a feed pH of 7.0 are given in Figs. 4 and 5. Fig. 4 gives results for AeDNV particles suspended in growth medium while Fig. 5 gives results for AeDNV particles suspended in water. In these figures the virus titre in the permeate is plotted as a function of permeate volume. As can be seen Q and D membranes successfully adsorb virus particles from both growth medium and water. However, few virus particles bind to C and S membranes for both feed streams at pH 7.0.

Breakthrough curves for the S membrane at a feed pH of 3.5 are shown in Fig. 6. As can be seen the virus titre in the growth medium and water are quite different. Adsorption of AeDNV is observed for viruses in water. However, no adsorption is observed for viruses in growth medium. Fig. 7 gives breakthrough curves for the C membrane at a feed pH of 4.7. The initial virus titre in the growth medium and the water was similar. For both feed streams it appears only a little non specific binding of AeDNV particles occurs.

Based on the results of Figs. 4–7, Table 2 gives the dynamic capacity of the membranes. The breakthrough volume was defined as the volume of feed solution that resulted

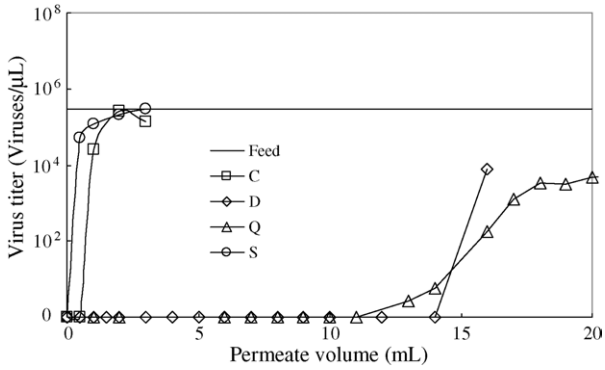

Fig. 5. Variation of the virus titre in the permeate with permeate volume. The feed consisted of virus particles suspended in water at pH 7.0. The feed flow rate was 1.0 mL/min. Results are shown for C, D, Q and S membranes.

Table 2
Summary of virus binding results

Membrane	pH	Virus charge	Membrane charge	Dynamic capacity			Static capacity
				Protein (mg)	Virus in water	Virus in medium	Virus in water
Q	7.0	Negative	Positive	60 (5.39×10^{17} molecules) BSA	$>2.79 \times 10^{10}$ viruses (1.96×10^{-4} mg)	$>1.36 \times 10^{10}$ viruses (9.59×10^{-5} mg)	6.2×10^{10} viruses (4.36×10^{-4} mg)
D	7.0	Negative	Positive	45 (4.04×10^{17} molecules) BSA	$>1.54 \times 10^{9}$ viruses (1.08×10^{-5} mg)	$>1.36 \times 10^{10}$ viruses (9.59×10^{-5} mg)	–
S	7.0	Negative	Negative	60 (2.53×10^{18} molecules) Lys	0	0	–
	3.5	Positive	Negative		$>3.91 \times 10^{8}$ viruses (2.74×10^{-6} mg)	0	–
C	7.0	Negative	Negative	45 (1.89×10^{18} molecules) Lys	0	0	–
	4.7	Positive	Negative		0	0	–

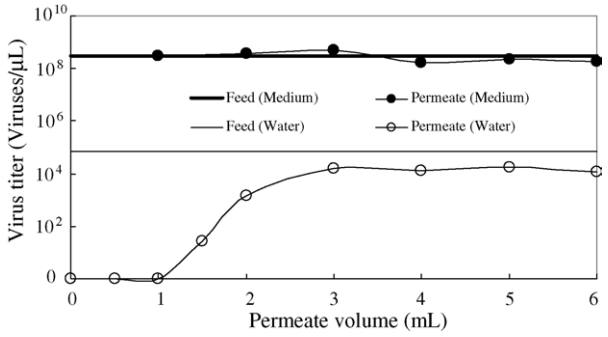

Fig. 6. Variation of the virus titre in the permeate with permeate volume for S membranes. The feed consisted of virus particles suspended in growth medium and water at pH 3.5. The feed flow rate was 1.0 mL/min.

in the permeate virus titre being 10% of the feed titre. The dynamic capacity of the membrane is given as the number of virus particles bound to a membrane surface area of 75 cm^2. Manufacturer's values for adsorption of BSA and lysozyme are also included. As can be seen the highest binding capacity is obtained for Q membranes loaded with viruses in water. Consequently we studied this system further by determining static binding data.

Fig. 8 gives the static binding results for Q membranes with a surface area of 25 cm^2 (or 0.69 mL) in 20 mL of water containing virus particles. The left hand side *y*-axis gives the virus titre in solution (denoted as open triangles) as a function of time while the right hand side *y*-axis gives the number of virus particles adsorbed per mL of membrane volume (denoted as crosses). The number of virus particles adsorbed onto the membrane was determined from the difference between the feed titre and the residual virus titre in solution. Based on these results the static binding capacity for Q membranes was determined. The result is also given in Table 2. The static binding capacity for Q membranes, incubated with viruses in water was determined at the same feed titre as used in the corresponding dynamic experiment shown in Fig. 5. In Table 2 binding capacities are given in units of virus particles per 75 cm^2 of membrane surface area in order to compare the results to the protein binding capacities given

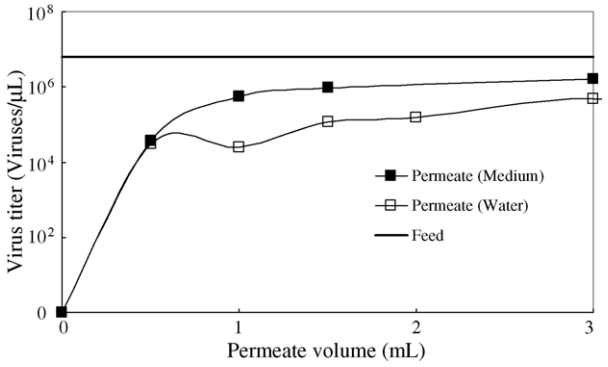

Fig. 7. Variation of the virus titre in the permeate with permeate volume for C membranes. The feed consisted of virus particles suspended in growth medium and water at pH 4.7. The feed flow rate was 1.0 mL/min.

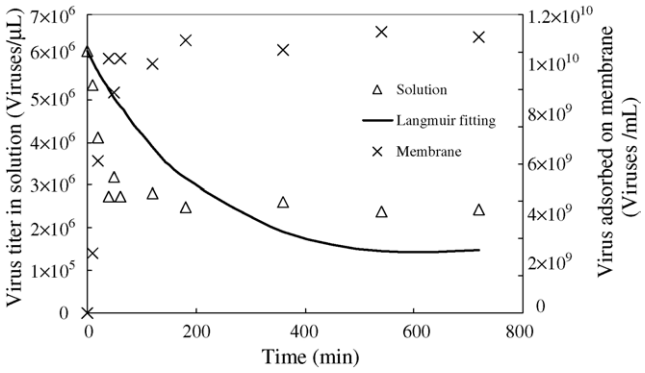

Fig. 8. Static adsorption results for Q membranes. The membrane surface area was 25 cm^2. Membranes were incubated in 20 mL of water containing virus particles at pH 7.0. The suspension was gently stirred at 290 rpm at 28 °C. The left hand side *y*-axis gives the virus concentration in solution as a function of incubation time while the right hand side *y*-axis gives the number of bound virus particles per mL of membrane volume. The continuous curve gives the Langmuir fitting results.

by the manufacturer. In Fig. 8 however, the units are virus particles adsorbed per volume of membrane. The membrane modules used in this work had a surface area of 75 cm^2 and a volume of 2 cm^3 as given by the manufacturer. Consequently, conversion between the units in Table 2 and Fig. 8 is routine.

Fig. 9 gives the adsorption isotherm for binding AeDNV to Q membranes. Results are plotted as the number of virus particles adsorbed per membrane volume versus the virus titre in solution (shown as open triangles). Fig. 9 was generated by incubating 25 cm^2 of Q membrane in 20 mL of water containing virus particles. Initial virus titres ranged from 10^4 to 10^8 viruses/μL at pH 7. The experiment was run for 24 h until equilibrium was reached. The temperature during adsorption was 28 °C.

By fitting the data shown in Fig. 9 to the single-solute Langmuir isotherm model (Eq. (2) with the left hand side equal to 0) the values of K_D and c_l were determined. Using these values of K_D and c_l, and the expression $K_D = k_d/k_a$, the data shown in Fig. 8 were fit to the Langmuir kinetic model (Eq. (2)) in order to determine the rate constants k_a and k_d [29]. The rate constants were found to be $k_a = 0.14\,(\text{mol/L})^{-1}\,\text{s}^{-1}$ and $k_d = 2.9 \times 10^{-5}\,\text{s}^{-1}$ and c_l was found to be 8.62×10^{-12} mol/m^2. The Langmuir fit is shown as a continuous curve in Figs. 8 and 9.

Fig. 10 compares the experimental and numerical breakthrough curves for Q membranes loaded with virus particles in water. In the simulation, viruses were assumed to be suspended in water at pH 7. In order to solve the set of partial differential Eqs. (2), (3) and (6)–(11), information about the membrane and the interactions between the virus and ion exchange groups is needed. The membrane pore size distribution is characterized using a log normal distribution. The log normal pore size is given by the following equation,

$$n(r) = n_0 \exp\left\{-\left[\frac{\log(r/3)}{\log 3}\right]^2\right\} \tag{12}$$

where n_0 is the number of pores at the maximum in the distribution function, which was estimated from SEM images to be 2×10^6 cm^{-2}. The tortuosity parameter was also estimated from SEM images of the membrane and found to be 1.4. During the simulation, Eq. (12) was discretized into a number of pore size ranges. An average pore size is used to describe each range. The percentage of pores in a given range is obtained by the fitted lognormal distribution. The concentration of virus particles leaving a given pore size range was calculated using Eqs. (2), (3) and (6)–(11). Then the average concentration of virus particles in the permeate was calculated by integrating the exit concentration of virus particle over the membrane surface. During the simulation, the physicochemical parameters for virus adsorption to ion exchange groups were obtained from the static binding results as described above. The virus diffusivity was estimated from Stokes-Einstein equation to be 3.5×10^{-12} m^2 s^{-1}. It can be seen from Fig. 10 that the numerical results correctly give the shape of the experimental breakthrough curve.

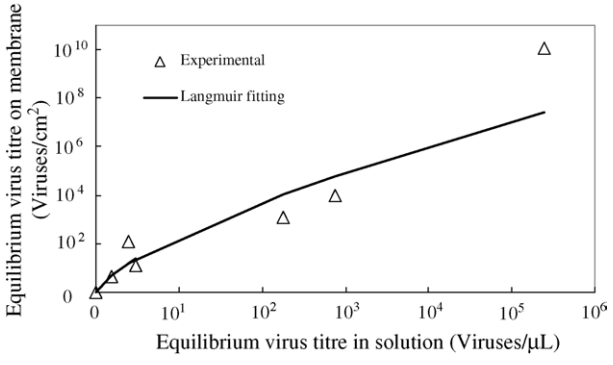

Fig. 9. Adsorption isotherm for Q membranes. The membrane surface area was 25 cm^2. Membranes were incubated in 20 mL water containing virus particles at pH 7.0. Initial virus titres in solution ranged from 10^4 to 10^8 viruses/μL. Experiments were run for 24 h at 28 °C. The continuous curve gives the Langmuir fitting results.

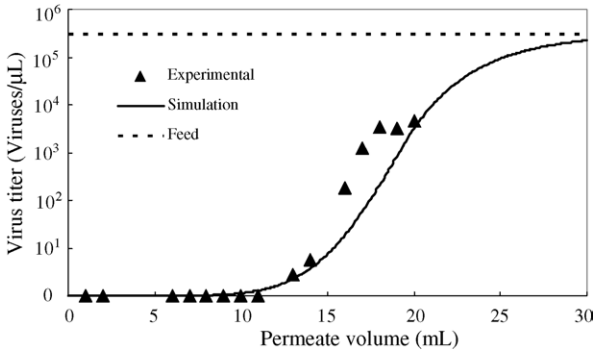

Fig. 10. Comparison of experimental and numerical results. Experimental results are for virus particles suspended in water at pH 7 pumped through Q membranes at 1 mL/min.

5. Discussion

Figs. 4 and 5 indicate that Q and D membranes are successful in adsorbing AeDNV particles. As shown in Table 1, the pK_a of the ion exchange groups for both membranes is much higher than 7.0. Consequently at a feed pH of 7.0, the ion exchange groups will be positively charged. Since the p*I* of AeDNV is 5.6, the virus particles will have an overall negative charge thus virus particles will be adsorbed by electrostatic interaction.

The two cation exchange membranes (S and C) did not adsorb a significant number of virus particles at a feed pH of 7.0. As can be seen from Table 1, at pH 7.0, the ion exchange groups of both membranes are negatively charged. Since AeDNV particles also have an overall negative charge at pH 7.0, little adsorption is expected. This result suggests that if the feed pH were adjusted such that the virus and ion exchange groups were oppositely charged, adsorption of virus particles should occur.

Breakthrough experiments were conducted using S membranes at a feed pH of 3.5. At this pH the ion exchange groups of the membrane will be negatively charged while the virus particles will have an overall positive charge. Fig. 6 indicates that virus particles are adsorbed from water. However, little virus adsorption is observed from growth medium.

Selecting a feed pH at which the ion exchange groups on the C membrane carry an opposite charge to the virus particles is difficult as the pK_a and p*I* of the ion exchange groups and virus particles are similar. Experiments were conducted at a feed pH of 4.7. At this pH virus particles are expected to carry an overall positive charge. Further about 60% of the ion exchange groups are expected to be negatively charged. Nevertheless little adsorption is observed for virus particles suspended in growth medium and water. Since the surface of AeDNV particles is likely to contain a number of groups that have different pK_a values, for a feed pH within 1 pH unit of the p*I* of the entire virus particle, the virus particles may be only slightly positively charged. Further at pH 4.7, only about 60% of the binding sites on the membrane are negatively charged probably explaining the lack of significant virus adsorption.

AeDNV particles are particularly robust. The particles remain viable over a pH range of 1–12. Consequently depending on the p*I* of the virus and the other charged species such as amino acids that may be present, by adjusting the feed pH it may be possible to maximize adsorption of AeDNV particle and minimize adsorption of other charged species. While this approach is feasible for other parvoviruses such as minute virus of mice (MVM), an FDA model parvovirus [30], it is unlikely to work for pH sensitive viruses such as influenza virus [31].

The results of the breakthrough experiments are summarized in Table 2. The first column gives the membrane tested, while the next three columns give the feed pH and the sign of the net charge of the virus and ion exchange groups at the feed pH. The next column gives the manufacturer's stated static capacity for bovine serum albumin (BSA, p*I* 4.9, MW 67,000) and lysozyme (p*I* 11, MW 14,300) [32]. The static capacity is determined by the manufacturer by incubating the membrane in 10 mmol/L potassium phosphate buffer at pH 7.0 containing 2 mg mL^{-1} of protein. The next two columns give the number of virus particles adsorbed from growth medium and water in dynamic adsorption experiments. The dynamic capacity is given as the number of virus particles adsorbed onto a membrane area of 75 cm^2 in order to be consistent with the capacity for protein binding reported by the manufacturer. The final column gives the number of virus particles adsorbed onto a Q membrane in static adsorption experiments. Again 75 cm^2 membrane surface area has also been used as the basis, in order to compare static and dynamic capacities. These values represent the dynamic and static capacity of the membranes under the experimental conditions tested.

The experimental results obtained here indicate that for Q membranes, about twice as many AeDNV particles were adsorbed from water compared to growth medium. For S membranes, no virus particles were adsorbed from the growth medium but virus particles were absorbed from water. For virus particles in water (grown using mosquito larvae), the concentration of dissolved amino acids and proteins is very low compared to virus particles suspended in growth medium [33]. At pH 7.0, a large number of the amino acids present will be negatively charged. These amino acids could compete with the virus particles for positively charged binding sites on the membrane surface leading to lower virus adsorption from the growth medium compared to water. Similarly at pH 3.5, many of the amino acids will be positively charged. These positively charged amino acids could compete with virus particles for negatively charged binding sites on the membrane leading to little binding of virus particles. In addition, albumin present in the fetal bovine serum that is added to the growth medium has a p*I* of 4.9. Therefore, it can also compete with AeDNV particles for binding sites.

The experimentally determined dynamic capacities given in Table 2 are several orders of magnitude less than the manufacturers stated values for the static protein binding capacity. AeDNV particles are about 20 nm in size which is much larger than BSA and lysozyme. Thus it is likely that smaller pores in the membrane are not accessible to virus particles and that steric hindrance effects lead to lower binding capacities. From Table 2, it also can be seen that for Q membranes incubated with virus water solutions, the dynamic capacity is within a factor of 2.5 of the static capacity.

The focus of the present work was the determination of breakthrough curves for AeDNV. Nevertheless we have also investigated elution of virus adsorbed on to Q membranes. The experimental results indicate that the virus particles adsorbed on to membranes can be effectively eluted and recovered by using 0.5 mol/L NaCl solution.

Design of a practical adsorptive membrane module for virus adsorption will require optimization of the membrane pore size and pore size distribution in order to maximize virus binding [34]. Pores that are smaller than the diameter of the virus particles, 20 nm for AeDNV, are unavailable for virus

binding. Thus ion exchange groups in these pores will be wasted. The presence of very large pores could result in a radial virus concentration gradient within the pores which in turn could lead to early breakthrough of virus particles. This in turn will result in the entire module capacity not being used. The maximum pore-size that does not lead to the formation of radial concentration gradients may be estimated from the ratio of the characteristic time for radial diffusion within the pore to the characteristic time for adsorption of virus particles. The characteristic time for radial diffusion, τ_D, is given by,

$$\tau_D = R_p^2/E \tag{13}$$

where R_p and E are the pore radius and diffusion coefficient of the virus particle. The characteristic time for adsorption depends on the reaction mechanism. The characteristic time for adsorption of virus may be approximated by [34,35],

$$\tau_R = \frac{1}{(kR_{max})} \tag{14}$$

where k is the second order rate constant for adsorption (see Equation (1)) and R_{max} is the maximum virus binding capacity (mg/mL). The ratio τ_D/τ_R is the second Damköhler number, Da_{II} [34,35]. Da_{II} much less than one indicates that radial concentration gradients are negligible.

As the flow rate through the pores increases, the residence time for virus particles within the pores decreases. When the residence time in the largest pores approaches the characteristic time for adsorption, early breakthrough and a flow rate dependent dynamic capacity will be observed. The maximum feed flow rate, for which the dynamic capacity is independent of flow rate may be estimated by calculating the ratio of the residence time to the characteristic time for virus adsorption.

The mean residence time, τ, is given by V/Q where V is the total empty (pore) volume of the membrane and Q is the feed flow rate. The characteristic time for virus adsorption is given by Eq. (14). The ratio of τ/τ_R is the first Damköhler number, Da_I. Thus, $Da_I > 1$ indicates that the characteristic adsorption time is less than the residence time in the pores.

Table 3 gives the first and second Damköhler numbers calculated using Eqs. (13) and (14) for the experiments conducted here. In Eq. (14), the product of kR_{max} (0.00025 /s) was calculated based on the Q membrane results in Fig. 5 using the method described by Unarska et al. [36]. The value of Da_I indicates that the rate of adsorption is fast compared to the average residence time. Further the value of Da_{II} indicates that radial concentration gradients within the larger pores are not significant.

Fig. 10 shows that the breakthrough curve for Q membranes from virus water feed solutions may be predicted using the model developed here. In Fig. 10, experimental results are shown for a total permeate volume of 20 mL while model predictions are shown for a permeate volume up to 30 mL. As can be seen, in the range 15–20 mL, the agreement between the experimental and calculated results is not as good as in the range 0–15 mL permeate. Experimental results were not obtained for permeate volumes higher than 20 mL, since in practical applications the process will not be run to bed exhaustion.

Table 3
Da_I and Da_{II} for AeDNV adsorption

τ_D (s)	τ_R (s)	τ (s)	Da_I	Da_{II}
0.4	3.1	43	14	0.13

While the numerical results correctly give the shape of the experimental breakthrough curve, deviations between the two are observed. The actual quantitative agreement between the experimental data and the Langmuir model may be determined by calculating the relative error defined as,

$$\text{Relative error} = \frac{(\text{Experimental result} - \text{Langmuir fit})}{\text{Experimental result}} \times 100\% \tag{15}$$

The relative errors are between −91 and 40% for data shown in Fig. 8 and −55 and 91% for data shown in Fig. 9. This poor quantitative agreement could be due to the accuracy of the RT-PCR assay used and the limited number of experimental data points. However, although the deviation between the experimental results and the Langmuir model are significant, a similar level of deviation has been reported by other researchers [32]. Further the model prediction depends upon fitting a Langmuir isotherm to the static binding data. A more complex isotherm expression, containing more parameters could be used to better describe the actual binding of virus particles to the ion exchange membrane [37–40]. However, given the accuracy of the virus assay, using a more complicated adsorption expression is not justified. Consequently, in keeping with early studies on adsorption of large biomolecules, the Langmuir isotherm is used here [37–41].

The analysis presented here uses Eq. (6) to predict the breakthrough curve for AeDNV in water loaded on to Q membranes. Thomas [42] solved Eq. (6) analytically by ignoring the diffusion term. Suen and Etzel [29] used the Thomas model as a basis for comparison of the effects of parameters such as axial diffusion and association kinetics on the breakthrough curve. While the approach presented here is also based on the Thomas model, there are some important differences. The model is being applied here to the breakthrough of virus particles. Though many studies have considered protein binding and elution [10–14], few studies have considered adsorption of virus particles.

The presence of a pore size distribution and variation of membrane thickness can have a very significant effect on the dynamic capacity of adsorptive membranes [29]. Unlike the Thomas model which assumes a uniform pore size, a log normal pore size distribution is fitted to SEM images of the membrane. Consequently, the liquid velocity through the pores is not equal but depends on the pore size. In addition, in

our model a tortuosity parameter is introduced to describe the effects of pore tortuosity and connectivity. Tortuosities ranging from 2 to 12 have been reported [43,44]. Further though the effects of axial diffusion are likely to be minor under the experimental conditions considered here, the axial diffusion term is retained in Eq. (6) as it is likely to be significant under some conditions.

The model presented here may be extended to calculate virus adsorption from growth medium onto Q membranes. In this case static adsorption data analogous to that shown in Figs. 8 and 9 will be required to determine the maximum binding capacity and the rate constants for adsorption and de-sorption. The model may further be extended to D and S membranes. In this case, in addition to static adsorption date, if the pore size distribution is different to Q membranes, SEM data will also be required.

The analysis described here ignores the effects of other components in the feed solution, such as amino acids that could compete with the virus particles for ion exchange sites. While the general mass transfer model is similar, incorporation of the effects of competitive binding will require the use of a more complex multi-component adsorption model for Eq. (2). Further, in order to estimate the additional parameters needed for other components, experiments will have to be conducted where the concentration of the competing species is varied. This will be difficult for virus particles suspended in growth medium. However, as is the case here, for virus particles suspended in water with a very low concentration of amino acids and proteins, the effects of competitive binding may be ignored.

6. Conclusions

Anion and cation exchange membranes have been used to adsorb AeDNV particles. Since the virus particles are viable over a large range of pH values, adjustment of the feed pH below and above the p*I* of the virus particles leads to positively and negatively charged particle respectively. Consequently, cation and anion exchange membranes may be used to adsorb the virus particles. The results obtained here indicate that adsorptive membranes may be ideally suited for virus capture as the effects of hindered pore diffusion are absent. Optimizing the membrane pore size and pore size distribution is likely to be very important in the design of practical adsorptive membranes for virus capture. A model is proposed describes the breakthrough curve for Q membranes in the absence of competition for binding sites by other negatively charged species.

Acknowledgements

Membranes were provided by Sartorius AG. Financial support was provided by the National Science Foundation (CAREER Program Grant No. BES 9984095), and the National Institutes of Health (AI 25489). The authors wish to thank Dr. Boris Afanasiev and Mr. Mark Flipse for their assistance.

References

[1] W. Berthold, J. Walter, W. Werz, Cytotechnology 9 (1992) 189.
[2] R. Valdés, N. Ibarra, I. Ruibal, A. Beldarraín, E. Noa, N. Herrera, R. Alemán, S. Padilla, J. Garcia, M. Pérez, R. Morales, E. Chong, B. Reues, Y. Quiñones, A. Agraz, L. Herrera, J. Biotechnol. 96 (2002) 251.
[3] P.L. Roberts, C.P. Walker, P.A. Feldman, Vox Sanguinis 67 (1994) 69.
[4] I.S. Kim, Y.W. Choi, S.R. Lee, H.S. Woo, S. Lee, J. Microbiol. Biotechnol. 11 (2001) 497.
[5] L.A. Dowing, J.M. Bernstein, A. Walter, J. Virol. Methods 38 (1992) 215.
[6] A. Carlsson, J. Kuznar, M. Varga, E. Everitt, J. Virol. Methods 47 (1994) 27.
[7] L. Walin, R. Tuma, G.J. Thomas, D.H. Bamford, Virology 201 (1994) 1.
[8] A. Karger, B. Bettin, H. Granzow, T.C. Mettenleiter, J. Virol. Methods 70 (1998) 219.
[9] P.A. Belter, E.L. Cussler, W.S. Hu, Bioseparations Downstream Processing for Biotechnology, Wiley, New York, 1988.
[10] R. Ghosh, J. Chromoatogr. A 952 (2002) 13.
[11] E. Klein, J. Membr. Sci. 179 (2000) 1.
[12] D.K. Roper, E.N. Lightfoot, J. Chromatogr. A 702 (1995) 3.
[13] J. Thömmes, M.R. Kula, Biotechnol. Prog. 11 (1995) 357.
[14] X. Zeng, E. Ruckenstein, Biotechnol. Prog. 15 (1999) 1003.
[15] F. Blanche, Amersham Biosci. Downstr. 27 (1999) 16.
[16] B.D. Kelley, M. Tannatt, R. Magnusson, S. Hagelberg, J. Booth, Biotechnol. Bioeng. 87 (2004) 400.
[17] A. Morrica, C. Nardini, A. Falbo, A.C. Bailey, E. Bucci, Biologicals 31 (2003) 165.
[18] W.S.W. Ho, K.K. Sirkar, Membrane Handbook, van Nostrand Reinhold, New York, 1992.
[19] W.K. Wang, Membrane Separations in Biotechnology, Marcel Dekker Inc., New York, 2001.
[20] H. Yang, C. Viera, J. Fischer, M.R. Etzel, Ind. Eng. Chem. Res. 41 (2002) 1597.
[21] H.L. Knudsen, R.L. Fahrner, Y. Xu, L.A. Norling, G.S. Blank, J. Chromatogr. A 907 (2001) 145.
[22] M.A. Teeters, S.E. Conrardy, B.L. Thomas, T.W. Root, E.N. Lightfoot, J. Chromatog. A 989 (2003) 165.
[23] M.S. Levy, R.D. O'Kennedy, P. Ayazi-Shamlou, P. Dunnill, Trends Biotechnol. 18 (2000) 296.
[24] C. Haber, J. Skupsky, A. Lee, R. Lander, Biotechnol. Bioeng. 88 (2004) 26.
[25] J.O. Carlson, B.N. Afansiev, S. Higgs, T. Matsubara, J.C. Burns, in: J.M. Crampton, C.B. Beard, C. Louis (Eds.), The Molecular Biology of Insect Disease Vectors: A Methods Manual, Chapman & Hall, New York, 1997.
[26] B.N. Afanasiev, Y.V. Kozlov, J.O. Carlson, B.J. Beaty, Exp. Parasitol. 79 (1994) 322.
[27] T.W. Ward, M.S. Jenkins, B.N. Afanasiev, M. Edwards, B.A. Duda, E. Suchman, M. Jacobs- Lorena, B.J. Beaty, J.O. Carlson, Insect Mol. Biol. 10 (2001) 397.
[28] J.P. Ledermann, E.L. Suchman, W.C. Black IV, J.O. Carlson, J. Econ. Entomol. 97 (2004) 1827.
[29] S.Y. Suen, M.R. Etzel, Chem. Eng. Sci. 47 (1992) 1355.
[30] F.A. Murphy, C.M. Fauquet, D.H.L. Bishop, S.A. Ghabrial, A.W. Jarvis, G.P. Martelli, M.A. Mayo, M.D. Summers, Virus Taxonomy, Sixth Report of the International Committee on Taxonomy of Viruses, Springer-Verlag, New York, 1995.

[31] A.R. Neurath, B.A. Rubin, W.A. Pierzchala, Arch. Biochem. Biophys. 120 (1967) 238.
[32] S.Y. Lin, S.Y. Suen, J. Membr. Sci. 204 (2002) 37.
[33] Mediatech, Inc. 2004. see: http://www.cellgro.com/tech2/msds_table.cfm.
[34] C. Charcosset, Z. Su, S. Karoor, G. Daun, C.K. Colton, Biotechnol. Bioeng. 48 (1995) 415.
[35] J.P. Catchpole, G. Fulford, Ind. Eng. Chem. 58 (1966) 46.
[36] M. Unarska, P.A. Davies, M.P. Esnouf, B.J. Bellhouse, J. Chromatogr. 519 (1990) 53.
[37] F.H. Arnold, H.W. Blanch, C.R. Wilke, Chem. Eng. J. 30 (1985) B9.
[38] K.H. Gebauer, J. Thömmes, M.R. Kula, Chem. Eng. Sci. 52 (1997) 405.
[39] S.-Y. Suen, J. Chem. Tech. Biotechnol. 65 (1996) 259.
[40] K. Al-Malah, H.A.H. Mousa, in: J. Tóth (Ed.), Adsorption—Theory, Modeling, and Analysis, Marcel Dekker, Inc., New York, NY, 2002, p. 847.
[41] H.A. Chase, J. Chromatogr. 297 (1984) 179.
[42] H.C. Thomas, J. Am. Chem. Soc. 66 (1944) 1664.
[43] Q. Zhang, E.L. Cussler, J. Membr. Sci. 23 (1985) 333.
[44] E.L. Cussler, Diffusion: Mass Transfer in Fluid Systems, Cambridge University Press, New York, NY, 1984.